Separation and Complete Analyses of the Overlapped and Unresolved ^{1}H NMR Spectra of Enantiomers by Spin Selected Correlation Experiments

Uday Ramesh Prabhu,† Bikash Baishya,† and N. Suryaprakash*,‡

Solid State and Structural Chemistry Unit, and NMR Research Centre, Indian Institute of Science, Bangalore 560 012, India

Received: October 23, 2007; Revised Manuscript Received: January 11, 2008

NMR spectroscopic discrimination of optical enantiomers is most often carried out using ^{2}H and ^{13}C spectra of chiral molecules aligned in a chiral liquid crystalline solvent. The use of proton NMR for such a purpose is severely hindered due to the spectral complexity and the significant loss of resolution arising from numerous short- and long-distance couplings and the indistinguishable overlap of spectra from both *R* and *S* enantiomers. The determination of all the spectral parameters by the analyses of such intricate NMR spectra poses challenges, such as, unraveling of the resonances for each enantiomer, spectral resolution, and simplification of the multiplet pattern. The present study exploits the spin state selection achieved by the two-dimensional ^{1}H NMR correlation of selectively excited isolated coupled spins (Soft-COSY) of the molecules to overcome these problems. The experiment provides the relative signs and magnitudes of all of the proton−proton couplings, which are otherwise not possible to determine from the broad and featureless one-dimensional ^{1}H spectra. The utilization of the method for quantification of enantiomeric excess has been demonstrated. The studies on different chiral molecules, each having a chiral center, whose spectral complexity increases with the increasing number of interacting spins, and the advantages and limitations of the method over SERF and DQ-SERF experiments have been reported in this work.

Introduction

The enatiomeric discrimination by NMR spectroscopy is a well-established tool.[1,2] Deriving this information from the isotropic solutions using chiral derivatizing agents is not routinely feasible. This problem has been circumvented by employing weakly aligned chiral liquid crystalline medium as an alternate methodology.[3] The diastereomeric interaction of the *R* and *S* enantiomers with the chiral liquid crystalline solvent produces a differential ordering effect. Unlike in thermotropic liquid crystals, the molecules in chiral liquid crystals are weakly ordered, and the orientational parameters are in the range of 10^{-3} to 10^{-5}. Nevertheless, it has a significant effect on the order-sensitive NMR spectral parameters like dipolar couplings (D_{ij}), quadrupolar couplings (Q_i), and chemical shift anisotropies ($\Delta\sigma_i$). This phenomenon has been exploited not only for enantiomeric discrimination but also to quantify their excess (ee). On the basis of the relative strengths of interactions, the sensitivity of anisotropic interactions to the differential ordering effect can be broadly classified in the decreasing order as quadrupole couplings, dipolar couplings, and the chemical shift anisotropies ($Q_i > D_{ij} > \Delta\sigma_i$). Therefore the majority of the reported work in the literature makes extensive application of ^{2}H NMR detection, exploiting the relatively large strengths of quadrupole couplings. There are several one- and two-dimensional experiments reported for such a purpose using deuterium in its natural abundance.[2–8] Needless to say, due to inherent low sensitivity because of its low natural abundance, these methods demand a large amount of the sample and enormous instrument time, which may not be feasible always. While dealing with other NMR-active spin 1/2 nuclei, the dipolar couplings and the chemical shift anisotropies are the obvious choice. As far as the employment of ^{13}C detection in its natural abundance is concerned, the possibility of detecting coupling between the dilute ^{13}C spins is 1 in 10^{-4}, and hence, the differential values of heteronuclear dipolar couplings and the chemical shift anisotropies have been exploited.[9,10] There are also studies using other nuclei like ^{19}F.[11,12]

With high magnetic moment, high natural abundance, and abundant presence in all of the chiral organic molecules ^{1}H detection is always advantageous. Furthermore, the proton detection requires less experimental time, and the errors on the estimation of enantiomeric excess are reported to be less compared to the detection of other NMR-active nuclei like ^{13}C and ^{2}H.[13] Although there are exceptions, the magnitudes of $\Delta\sigma_i$ of the protons are small even in strongly aligned thermotropic liquid crystals.[14] In the weakly aligned chiral liquid crystals, the immeasurably smaller value of this parameter results in indistinguishable overlap of transitions from both of the enantiomers. Thus, it is imperative that proton $\Delta\sigma_i$ cannot be exploited as an indicator for enantiomeric discrimination. Nevertheless, we have combated this problem and recently developed a method using chemical shift anisotropy as an exclusive parameter for the complete unraveling of the ^{1}H NMR spectra of enantiomers by employing the homonuclear highest quantum coherence.[15] The method provided a single transition for each enantiomer in the higher quantum dimension, at their respective cumulative additive value of $\Delta\sigma_i$ of all of the coupled protons. The cross sections taken parallel to the SQ dimension at each of these two resonance frequencies provided an enantiopure spectrum. As far as the utilization of proton−proton dipolar couplings is concerned, there are several experimental schemes reported in the literature to visualize enantiomers.[16–22] However, there is very little reported work on the complete

* To whom correspondence should be addressed. E-mail: nsp@sif.iisc.ernet.in. Fax: 0091 80 23601550. Tel: 0091 80 22933300.
† Solid State and Structural Chemistry Unit.
‡ NMR Research Centre.

10.1021/jp7102462 CCC: $40.75
Published on Web 05/30/2008

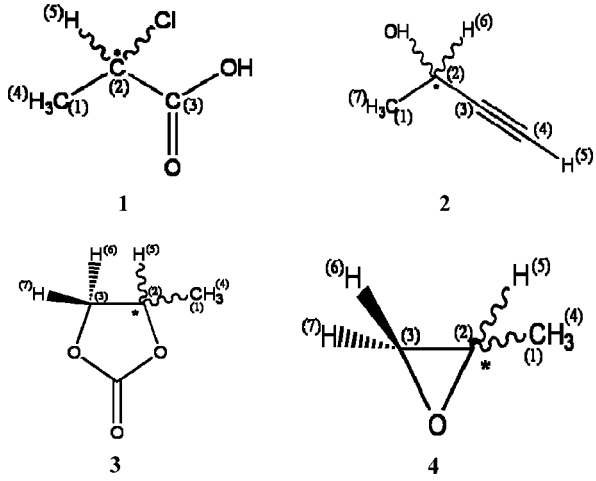

Figure 1. The racemic structures and the numbering of interacting spins of (**1**) (*R*/*S*)-2-chloropropanoic acid, (**2**) (*R*/*S*)-3-butyn-2-ol, (**3**) (*R*/*S*)-propylene carbonate, and (**4**) (*R*/*S*)-propylene oxide.

analyses of the proton spectra and the determination of the relative signs and magnitudes of the proton−proton couplings.[1,21]

We have been focusing our attention on the methodological developments to circumvent the problems and limitations in employing ^{1}H detection. Our recently proposed double quantum excited selective refocusing (DQ-SERF) method[23] results in better chiral visualization and has been demonstrated to be superior over the well-known SERF experiment. Furthermore, we were able to detect long-range couplings also in the direct dimension in addition to chiral discrimination in the indirect dimension. The present study focuses on the spin-selected correlation experiments (Soft-COSY),[24–26] which exploit the separation of the active and passive couplings achieved by the two-dimensional ^{1}H NMR correlation of a selectively excited isolated group of coupled spins. The experiment provides unambiguous enantiomeric visualization and spectral simplification and aids in the complete determination of all of the proton−proton couplings. This is demonstrated on four different chiral molecules, each having a chiral center, whose ^{1}H spectral complexity increases with the increase in the number of interacting spins. The relative signs and magnitudes of all of the proton−proton couplings have been determined from the broad and featureless ^{1}H spectra. The advantages and limitations of the Soft-COSY experiment compared to those SERF and DQ-SERF have also been discussed.

Experimental Confirmation

For the demonstration of the experimental technique, four different molecules, (*R*/*S*)-2-chloropropanoic acid (**1**), (*R*/*S*)-3-butyn-2-ol (**2**), (*R*/*S*)-propylene carbonate (**3**), and (*R*/*S*)-propylene oxide (**4**), were chosen. The samples were purchased from Sigma and used without further purification. The racemic structures and the numbering of the interacting spins of these molecules are given in Figure 1. The samples were prepared by the method described in the literature.[8,20] For the oriented sample **1**, 50 mg of the racemic mixture, 80 mg of poly-γ-benzyl-L-glutamate (PBLG) with DP 782 procured from Sigma, and 580 mg of $CDCl_3$ were used. For oriented sample **2**, 85 mg of PBLG, 59 mg of racemic mixture of **2**, and 450 mg of $CDCl_3$ were used. To explore the possibility of measuring ee, the scalemic (with 18.5% ee of *S* enantiomer) mixture of **2** was also prepared with 29 mg of *R* enantiomer and 42.2 mg of *S* enantiomer, 90 mg of PBLG, and 614 mg of $CDCl_3$. For the oriented sample **3**, 54 mg of the racemic mixture of **3**, 102.8 mg of PBLG, and 665 mg of $CDCl_3$ were used. Another scalemic (with 21.1% ee of *S* enantiomer) mixture of sample **3** with 28.0 mg of *R* enantiomer and 43 mg of *S* enantiomer, 123.0 mg of PBLG, and 650.0 mg of $CDCl_3$ were used. For the oriented sample **4**, 42.5 mg of racemic mixture of **4**, 78 mg of PBLG, and 580 mg of $CDCl_3$ were used. The samples were sealed in a 5 mm NMR tube to avoid the evaporation of the solvent and then centrifuged back and forth for several hours until the visually homogeneous phase was observed. The one- and two-dimensional proton spectra of all of the molecules were recorded using a Bruker DRX-500 NMR spectrometer. The temperature was maintained at 300 K for all of the samples using Bruker BVT 3000 temperature controller unit. The alignment of each sample was investigated by monitoring the ^{2}H doublet separation of $CDCl_3$. The one-dimensional ^{1}H spectra of all of the molecules along with the assignment of peaks to different protons, taken from the literature,[1,17,19,20] are given in Figure 2. The spectra display the increasing order of the complexity from the bottom trace to the top trace. The assignment of peaks for enantiomers *R* and *S* is normally carried out by recording the spectrum of an enantiopure sample and then comparing it with the spectrum of a racemic/scalemic mixture. For all of the molecules, the assignments for *R* and *S* enantiomers were taken from the literature. Although the parameters are not exactly the same, compared to earlier experiments, the same assignments were maintained. This assumption is reasonable as the spectral appearances do not differ drastically. In **2**, although our values are substantially different from the reported values,[1] adapting the trend from the earlier work, the enantiomer with a larger coupling among methyl protons has been assigned to the *R* enantiomer.

The pulse sequence for selective excitation is well-known[24–26] and is therefore not given. Unlike in nonselective 90° COSY experiments, in the present experiments, the soft 90° pulses are applied to the chosen isolated group of coupled spins. We have carried out two different types of selective correlations experiments, one on the isolated methyl resonance in all of the chosen molecules using a single selective pulse and the other the single or biselective excitation of different coupled spins in **2**, **3**, and **4**. The selective pulses were SEDUCE/EBURP-2/REBURP/UBURP shape pulses depending on the molecule and the type of experiments performed.

For a comparative study, SERF and DQ-SERF experiments were also carried out on all of the molecules. These experiments were, however, restricted to only selected excitation of isolated methyl groups, in addition to the selective excitation of protons numbered 5 and 7 for Soft-COSY and SERF in **3**. It may be pointed out that in the original SERF experiment, the enantiomeric discrimination was visualized in the indirect dimension using only the geminal couplings among the methyl protons, and the long-range couplings were not detected. In our reported work,[23] we have demonstrated that with careful experimentation, the SERF pulse sequence yields additional information in the direct dimension on the long-range couplings between the selectively excited methyl protons and the passive spins. Furthermore, we have also demonstrated that the biselective pulses were not essential for the methyl-proton-excited SERF experiment.

The acquisition and processing parameters employed in all of the 2D experiments are reported in the corresponding figure captions. The important difference to be highlighted is the optimization of the τ delay in the DQ-SERF experiment, which has already been extensively discussed.[23]

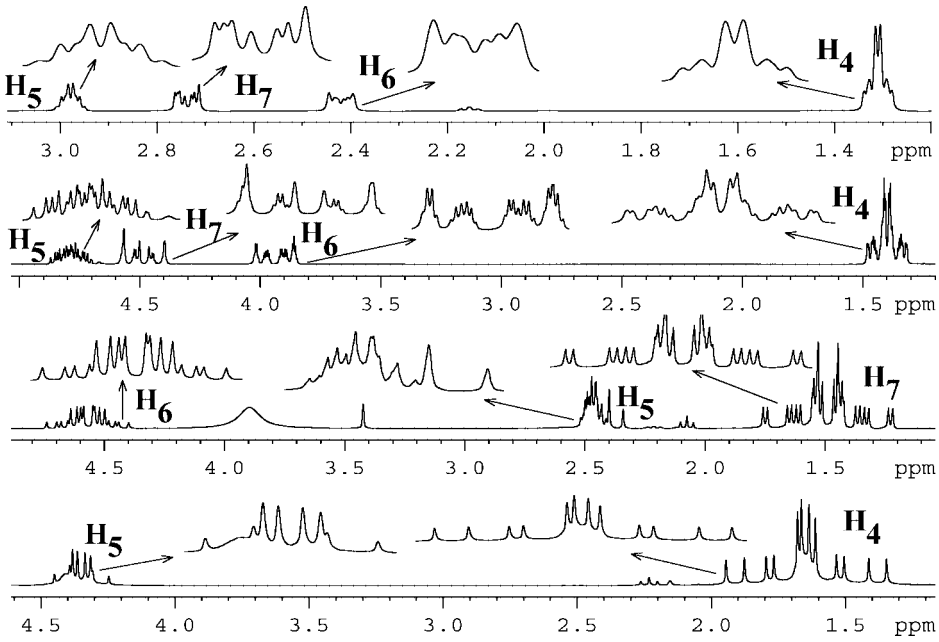

Figure 2. From bottom trace to top trace: 500 MHz one-dimensional ^{1}H spectrum of (*R*/*S*)-2-chloropropanoic acid, (*R*/*S*)-3-butyn-2-ol, (*R*/*S*)-propylene carbonate, and (*R*/*S*)-propylene oxide. The expanded regions of each spectrum and the assignment to different protons are shown. Chemical shifts were referenced with the isotropic value of methyl protons.

Spin-Selective Correlation Experiments. In the experiments involving the application of selective pulses, the selectively excited spins are called active spins, and the remaining spins are called passive spins. In selectively excited experiments on homonuclear spins, the passive spins mimic the heteronuclei. Consequently, in the 2D selectively excited correlation experiments, there are several advantages: (a) separation of active and passive couplings in two dimensions, (b) reduced multiplicity compared to a normal COSY spectrum, (c) a reduction in the experimental time by several orders of magnitude, and (d) higher resolution because of the reduced spectral width chosen.[27] Thus, the experiment reveals several aspects of the spectrum which are otherwise not possible to derive from the normal broad and featureless one-dimensional spectrum. Furthermore, there is an enhanced resolution in each cross section taken parallel to the F_2 dimension due to the fact that the states of the passive spins are not disturbed both in the F_1 and F_2 dimensions, and the COSY peaks are labeled according to their spin states. In a system with a single passive spin, the resonances of the active spins are split into a doublet in each dimension, and each component of this doublet corresponds to the spin state $|\alpha\rangle$ or $|\beta\rangle$ of the passive spin. As an example, in a simple three-spin system of the type AMX, where X is the passive spin, the normal COSY spectrum gives 16 peaks. In contrast, the selectively excited COSY, with a phase-sensitive detection, shows two antiphase peaks with splitting due to active coupling displaced by a vector representing the passive splitting in both dimensions. However, possibly due to numerous long- and short-distance couplings, the correction of phases of peaks in the phase-sensitive detection were problematic, and hence, all of the spectra were reported in the magnitude. Nevertheless, the F_2 dimension reveals the coupling between the active spins, and the displacement of arrays in the F_1 dimension reveals the passive couplings. This is also a significant advantage as the spectrum is drastically simplified in each cross section, aiding the analysis. Another interesting feature of this experiment is that the cross-peak multiplicity pattern is similar to that of an E-COSY spectrum,[28,29] and hence, it is possible to determine the relative signs of the couplings whether the spins are scalar- or dipolar-coupled as long as the first-order analyses of the spectra are possible. In the subsequent sections, the analyses of the spectra of all of the molecules shown in Figure 2 will be discussed with the increasing order of the spectral complexity.

Results and Discussion

In **1**, **2**, **3**, and **4**, the resonances of different groups of protons are well isolated. In both **1** and **2**, the hydroxyl proton did not couple to the remaining protons. In **3** and **4**, each proton shows sizable coupling with the remaining protons, and the peaks show excessive remote coupling-assisted broadening, in addition to indistinguishable overlap of the spectra of both of the enantiomers. With the spectrum of each molecule being first order, despite the fact that A_3 spin systems are strongly coupled, the nomenclature of the spin system used for the analyses of the spectra similar to that of the liquid state spectra can be employed.

Analyses of the Spectra of (*R*/*S*)-2-Chloropropanoic Acid (1). In **1**, the coupled protons form a weakly coupled spin system of the type A_3X, where the A_3 group pertains to methyl protons and X is the methine proton. The first-order analysis of the spectrum is straightforward. The methyl proton resonance is split into a 1:2:1 triplet due to residual dipolar couplings among the magnetically equivalent protons. The separations which provide coupling information are designated as $^nT_{HH}$, where superscript n refers to protons that are n bonds away. Thus, the separation between the adjacent transitions of the triplet provides $^2T_{HH}$ (= $3D_{HH}$, between the methyl protons). Each component of the triplet is further split into a doublet of equal intensity due to coupling with the methine proton, providing $^3T_{HH}$ (coupling between methyl protons and the methine proton). This can be construed as two A_3 subspectra. Similarly, the methine proton is a quartet due to its coupling with methyl protons. The spectrum is a mixture of two such spectra arising from two enantiomers.

The two-dimensional selective methyl-proton-excited COSY spectrum of **1** is shown in Figure 3. The 2D spectrum displays two groups of transitions with different coupling strengths. Each

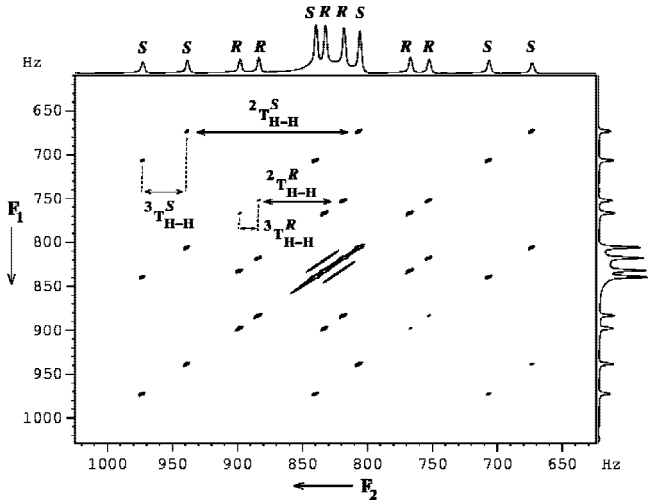

Figure 3. The 500 MHz two-dimensional correlation spectra of the selectively excited methyl group in (*R*/*S*)-2-chloropropanoic acid along with F_1 and F_2 projections. The width of the seduce shape pulse is 2.5 ms. The size of the 2D data matrix is 512 × 1402. Spectral widths are 500.0 and 500.0 Hz in the F_1 and F_2 dimensions. The number of accumulations for each t_1 increment is 8. The relaxation delay is 2.5 s. The data was zero-filled to 2048 and 4096 and processed with a sine bell window function. The digital resolution in the F_1 and F_2 dimensions is 0.24 and 0.12 Hz. Assignments for *R* and *S* are taken from the literature.[19] The separations marked $({}^{n}T_{HH})^{R/S}$ provide coupling information.

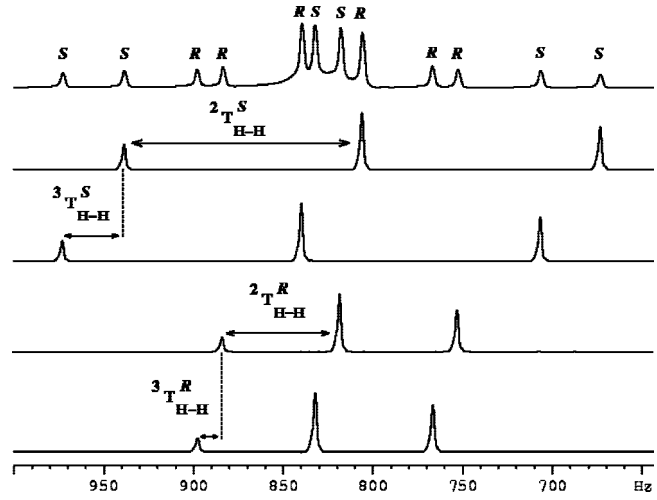

Figure 4. The first two cross sections for each enantiomer of Figure 3 taken along the F_2 dimension. The separations of the adjacent transitions of the triplet provide active coupling $({}^{2}T_{HH})^{R/S}$ and the displacements shown by broken lines provide the passive coupling $({}^{3}T_{HH})^{R/S}$.

group has six arrays of triplets of identical active coupling. Each group of this array of triplets pertains to one enantiomer. Clear separation of the group of triplets due to the differential ordering effect enables their unambiguous visualization. The cross section taken parallel to the F_2 dimension for each transition of *R* and *S* enantiomers directly provides $({}^{2}T_{HH})^{R/S}$, the active coupling information. The displacement of two consecutive cross sections of each enantiomer provides $({}^{3}T_{HH})^{R/S}$, the coupling between active and passive spins. The separations providing coupling information are marked in Figure 3. The spectral simplification by the separation of two A_3 subspectra is clearly visible from the plot of the two consecutive cross sections for each enantiomer of Figure 3, shown in Figure 4. The unambiguous discrimination of enantiomers is also clearly evident. With the spectra being symmetric with respect to the diagonal, similar information can be derived by analyzing the cross sections taken parallel to the F_1 dimension and the displacements in the F_2 dimension. The measured separations providing coupling information are given in Table 1.

Analyses of the Spectra of (*R*/*S*)-3-Butyn-2-ol (2). In **2**, the coupled protons (numbered 5, 6, and 7 in Figure 1) form a spin system of the type A_3MX, where A_3 (7) corresponds to methyl protons and M (6) and X (5) correspond to protons of the methine and acetylenic, groups respectively. The one-dimensional ^1H spectrum has well-resolved peaks for the CH_3 and two CH groups. The CH_3 group gives a triplet due to dipolar coupling among the magnetically equivalent protons. Each component of this triplet is further split into a doublet of a doublet due to four possible spin states $|\alpha\alpha\rangle$, $|\alpha\beta\rangle$, $|\beta\alpha\rangle$, and $|\beta\beta\rangle$ of the M and X spins. Thus, it displays 12 transitions corresponding to four A_3 subspectra. Similarly, each of the methine and acetylenic protons splits into a quartet due to the CH_3 group, and each component of the quartet is split into a doublet from the remaining single proton.

The selective methyl-group-excited COSY spectrum of **2** (racemic mixture) is reported in Figure 5. The active coupling is the dipolar coupling among methyl protons, and the passive couplings are between the methyl and the remaning two protons (5 and 6). The F_2 dimension results in 12 transitions for each enantiomer, construed as 4 A_3 subspectra, which are displaced in the F_1 dimension due to passive couplings. Each cross section pertains to an A_3 subspectra, which is a triplet, and the separations of the adjacent transitions, which provide $({}^{2}T_{H7H7})^{R/S}$. The separations marked with a, b, and c provide ${}^{n}T_{HH}$ (n = 2, 3, and 5) for the *R* enantiomer, and the separations d, e, and f provide similar information for the *S* enantiomer. The first four cross sections taken along the F_2 dimension for each transition of an enantiomer in the F_1 dimension is given in Figure 6, which depicts the complete separation of four A_3 subspectra of both the enantiomers. It may be pointed out that as far as the determination of ${}^{n}T_{HH}$ (n = 2, 3, and 5) is concerned, the first three cross sections are sufficient. Compared to a previously discussed molecule, the (*R*/*S*)-3-butyn-2-ol has additional couplings. Thus, the spectral complexity has increased in each dimension. The significant advantage of the spin-selected correlation experiment in spectral simplification, by separating the active and passive couplings in two dimensions, is clearly evident.

The coupling between the passive protons numbered 5 and 6 is not reflected either in the F_1 or in the F_2 dimension. This information is lacking for the determination of all of the couplings. Another experiment with the selective excitation of methine and acetylenic protons does provide this information along the F_2 dimension and the passive couplings to these protons in the F_1 dimension. The difficulty in such simultaneous excitation is their frequency separation, which is more than 1 kHz. The problem can, however, be combated by utilizing biselective pulses. The biselective methine- and acetelynic-proton-excited 2D spectrum along with the F_1 and F_2 projections is given in Figure 7A. The coupling information can be derived by the analyses of the cross-peaks multiplet pattern. The set of doublets due to coupling of active spins along the F_2 dimension is displaced in the F_1 dimension due to passive couplings of protons 5 and 6 with methyl protons. The expanded plot of the cross peaks for the methine proton (6) is given in Figure 7B. The passive coupling to proton 6, ${}^{3}T_{H6H7}$, results in a quartet. Each component of the quartet is further split into a doublet by another active coupling to proton 6, that is, ${}^{4}T_{H5H6}$. Thus, the

TABLE 1: Spectral Parameters (in Hz) Providing Information on the Different Couplings in 1, 2, 3, and 4 Aligned in Chiral Polypeptide Liquid Crystal PBLG

	(*R*/*S*)- 2-chloropropanoic		(*R*/*S*)-3-butyn-2-ol			(*R*/*S*)-propylene carbonate		(*R*/*S*)-propylene
parameter	acid	parameter	racemic mixture	scalemic mixture	parameter	racemic	scalemic	oxide
$(^2T_{HH})^R$	59.7	$(^2T_{H7H7})^R$	103.4	90.0	$(^2T_{H4H4})^R$	35.0	28.0	12.5
$(^3T_{HH})^R$	15.6	$(^3T_{H7H6})^R$	49.4	44.4	$(^3T_{H4H5})^R$	9.5	8.2	4.0
$(^2T_{HH})^S$	110.3	$(^5T_{H7H5})^R$	9.1	7.0	$(^4T_{H4H6})^R$	3.1	2.1	1.6
$(^3T_{HH})^S$	25.1	$(^4T_{H6H5})^R$	21.1	17.4	$(^4T_{H4H7})^R$	1.1	0.6	0.6
		$(^2T_{H7H7})^S$	88.4	36.7	$(^3T_{H5H6})^R$	25.7	20.5	8.5
		$(^3T_{H7H6})^S$	32.8	29.3	$(^3T_{H5H7})^R$	32.8	25.6	7.2
		$(^5T_{H7H5})^S$	9.3	6.9	$(^2T_{H6H7})^R$	52.7	35.5	14.4
		$(^4T_{H6H5})^S$	13.58	11.8	$(^2T_{H4H4})^S$	18.4	15.4	5.1
					$(^3T_{H4H5})^S$	13.8	11.4	6.7
					$(^4T_{H4H6})^S$	3.1	2.1	−1.4
					$(^4T_{H4H7})^S$	3.1	2.1	−0.22
					$(^3T_{H5H6})^S$	18.8	15.4	6.44
					$(^3T_{H5H7})^S$	24.4	19.5	5.1
					$(^2T_{H6H7})^S$	62.2	43.8	20.1

F_1 dimension gives two sets of identical quartets for each enantiomer displaced according to their coupling strengths. The separations marked with a, b, and c in Figure 7B provide $^4T_{H5H6}$, $^3T_{H7H6}$, and $^4T_{H5H7}$ for the *R* enantiomer, and the separations marked d, e, and f provide similar information for the *S* enantiomer. Thus, the totality of the coupling information could be obtained by the first-order analyses of the spectra without resorting to iterative analysis, unlike in a previous study on this molecule.[1] Furthermore, to establish the precision of the parameters, these values can be employed as the starting parameters for the iterative analyses, which aids in simplifying the iteration. This is another advantage.

Analyses of the Spectra of (*R*/*S*)-Propylene Carbonate and (*R*/*S*)-Propylene Oxide (3 and 4). In both **3** and **4**, the protons of the CH_2 groups are diastereotopic and have different chemical shifts. The coupled protons (numbered 4−7 in Figure 1) pertain to the spin system of the type A_3MNX, where A_3 (4) corresponds to methyl protons, M (6) and N (7) are methylene protons, and X (5) is the methine proton. As far as the splitting pattern of different protons is concerned, it is identical in both systems. The A_3 part of the spectrum gives rise to a triplet, each component of which is further split by methine and two diasterotopic methylene protons, giving rise to a total of 24 transitions. The spectral region of the methine proton is very complex, with coupling from methyl protons giving rise to a quartet, each component of which is further split into two doublets of equal intensity from two methylene protons. The complexity of the spectrum gets doubled due to a mixture of two spectra of enantiomers. It is evident from the expanded regions shown in Figure 2 that it is impossible to recognize any fine structure and extract meaningful information from these spectra. For the methyl group alone, there are 48 transitions overlapped in a narrow spectral width of nearly 70 Hz in **3** and within 40 Hz in **4**. The real challenge is not only to separate these overlapped spectra but also to extract the coupling information from the broad and featureless spectra. This emphasizes the necessity of an experiment to simplify the

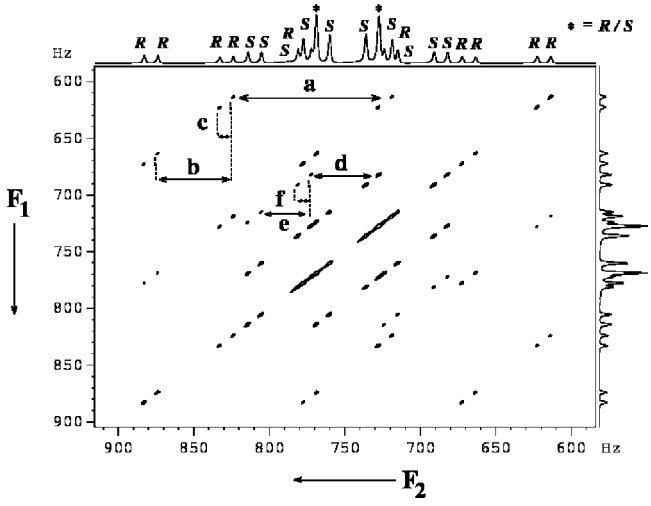

Figure 5. The 500 MHz two-dimensional correlation spectra of the selectively excited methyl resonance in a racemic mixture of (*R*/*S*)-3-butyn-2-ol along with the F_1 and F_2 projections. The width of the seduce shape pulse is 5 ms. The size of the 2D data matrix is 400 × 1602. Spectral widths are 350 and 442 Hz in the F_1 and F_2 dimensions. The number of accumulations for each t_1 increment is 4. The relation delay is 3.2 s. The data was zero-filled to 2048 and 4096 and processed with a sine bell window function. The digital resolution in the F_1 and F_2 dimensions is 0.17 and 0.10 Hz. Assignments for *R* and *S* are taken from the literature.[1] The separations marked with a, b, and c provide $^2T_{H7H7}$, $^3T_{H6H7}$, and $^5T_{H5H7}$ for the *R* enantiomer, and the separations d, e, and f provide $^2T_{H7H7}$, $^3T_{H6H7}$, and $^5T_{H5H7}$ for the *S* enantiomer. The peak marked * indicates the overlapped transitions from *R* and *S*. Notice the unambiguous enantiomer separation and the spectral simplification.

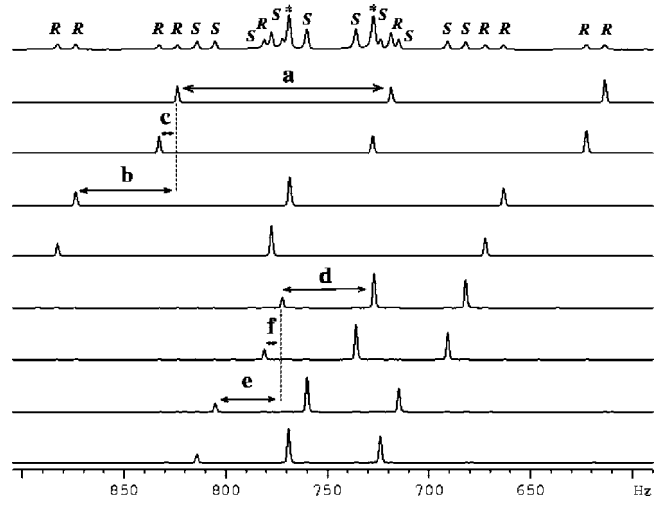

Figure 6. The first four cross sections for each enantiomer of Figure 5 taken along the F_2 dimension. The separations marked with a, b, and c provide $^2T_{H7H7}$, $^3T_{H6H7}$, and $^5T_{H5H7}$ for the *R* enantiomer, and the separations d, e, and f provide $^2T_{H7H7}$, $^3T_{H6H7}$, and $^5T_{H5H7}$ for the *S* enantiomer. Notice that the first three cross sections for each enantiomer are sufficient for the determination of all of the coupling information.

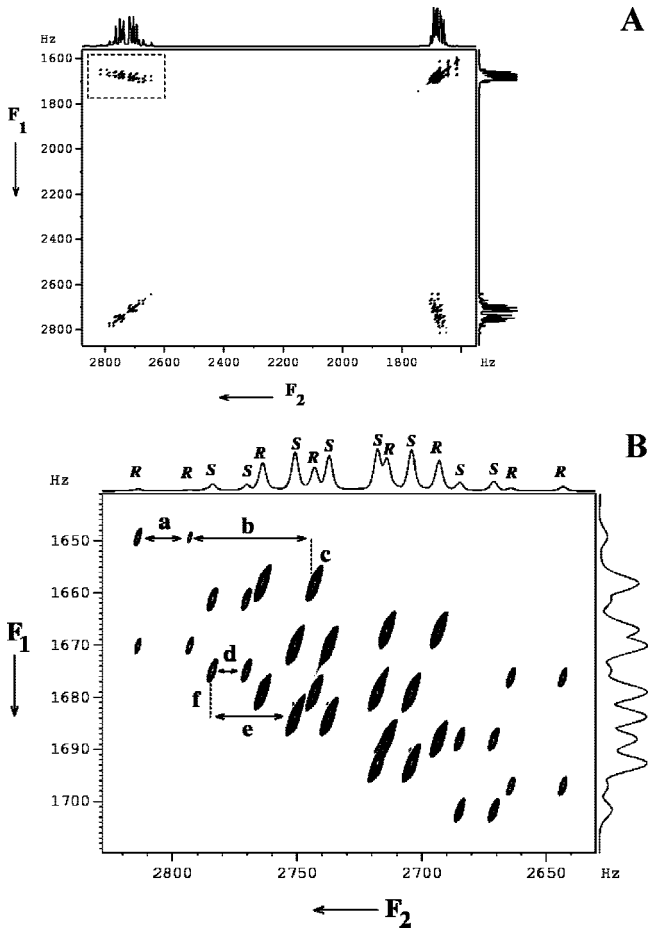

Figure 7. (A) The 500 MHz two-dimensional correlation spectra of simultaneous biselective excitation of methine (6) and acetylenic (5) resonances in a racemic mixture of (*R*/*S*)-3-butyn-2-ol, along with F_1 and F_2 projections. The width of the seduce shape pulse is 10 ms. The 2D data matrix is 1024 × 2840. Spectral widths are 1420 and 4096 Hz in the F_1 and F_2 dimensions. The number of accumulations for each t_1 increment is 4. The relaxation delay is 4.0 s. The data was zero-filled to 8192 and 4096 and processed with a sine bell window function. The digital resolution in the F_1 and F_2 dimensions is 0.34 and 0.17 Hz. (B) The expanded plot of cross peaks pertaining to proton 6, marked with a broken rectangle in A. The separations a, b, and c provide, respectively, $^4T_{H5H6}$, $^3T_{H6H7}$, and $^4T_{H4H7}$ for the *R* enantiomer, and those marked with d, e, and f provide, respectively, $^4T_{H5H6}$, $^3T_{H6H7}$, and $^4T_{H4H7}$ for the *S* enantiomer.

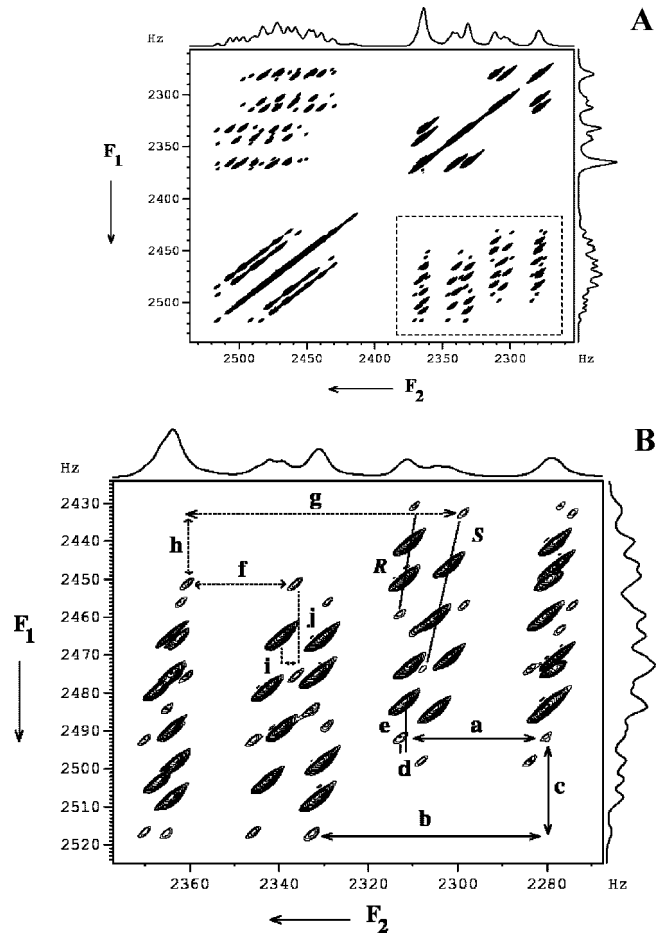

Figure 8. (A) The 500 MHz two-dimensional correlation spectra of biselective excitation of proton 5 (methine) and 7 (methylene) resonances in a racemic mixture of (*R*/*S*)-propylene carbonate along with F_1 and F_2 projections. The width of the seduce shape pulse is 5 ms. The 2D data matrix is 409 × 1024. Spectral widths are 350 and 448 Hz in the F_1 and F_2 dimensions. The number of accumulations for each t_1 increment is 4. The relaxation delay is 4.0 s. The data was zero-filled to 1024 and 4096 and processed with a sine bell window function. The digital resolution in F_1 and F_2 dimensions is 0.34 and 0.10 Hz. (B) Expanded plot of Figure 9A pertaining to cross peaks of proton 7 marked with a broken rectangle. The separations marked with solid arrows and represented by a, b, c, d, and e provide coupling information $(^3T_{H5H7})^S$, $(^2T_{H6H7})^S$, $(^4T_{H4H7})^S$, $(^3T_{H5H6})^S$, and $(^3T_{H4H5})^S$, whereas the separations marked with broken arrows and represented by g, h, i, j, and k provide $(^3T_{H5H7})^R$, $(^2T_{H6H7})^R$, $(^4T_{H4H7})^R$, $(^3T_{H5H6})^R$, and $(^3T_{H4H5})^R$. Note the resolution achieved and the quartet due to long-range coupling $(^4T_{H4H7})^R$ and $(^4T_{H4H7})^S$, displaced according to passive coupling in the F_1 dimension. One such quartet for each *R* and *S* enantiomer is shown by a cross line joining them.

analyses and obtain coupling information. The two-dimensional correlation experiments with a judicious choice of spins for selective excitation overcame these problems.

The comprehensive discussion on the analyses of the 2D spectra of **3** will be provided, and the same analogy is extended for the analyses of the 2D spectra of **4**. The 2D correlated spectrum of **3** (scalemic mixture) with selective excitation of the methyl protons is given in the top trace of Figure 11. The selective excitation of methyl protons leaves the two nonequivalent methylene protons and the methine proton as the passive spins. The 2D spectrum then pertains to the A_3 part of the A_3MNX spin system containing 24 transitions, which can be construed as 8 A_3 subspectra corresponding to 8 spin states of M, N, and X together, displayed in both direct and indirect dimensions, for each enantiomer. In the F_2 dimension, the active coupling is among the methyl protons and gives a triplet. Each component of this triplet is further split by the passive couplings from the remaining three M, N, and X protons and is displaced according to their coupling strengths. Thus, both the F_1 and F_2 dimensions must display two sets of A_3 subspectra, one for each enantiomer with distinctly different coupling strengths enabling their discrimination. However, experimentally, four A_3 subspectra for the *R* enantiomer and six A_3 subspectra for the *S* enantiomer were observed. This implies that long-distance couplings to methyl protons, namely, $^4T_{H4H6}$ and $^4T_{H4H7}$, are nearly equal for the *S* enantiomer and that one of the long-distance couplings is negligibly small in the *R* enantiomer. The cross section taken parallel to the F_2 dimension, at any one of the transitions of the subspectrum in the F_1 dimension, is a triplet which gives $(^2T_{H4H4})^{R/S}$ $(= 3 \times 2D_{HH})^{R/S}$, the coupling among the methyl protons. Furthermore, the displacement of cross sections along the F_1 dimension permits the measure of $(^nT_{HH})^{R/S}$ (where $n = 3$ and 4). The separations which provide information on different couplings are marked in top trace of Figure 11.

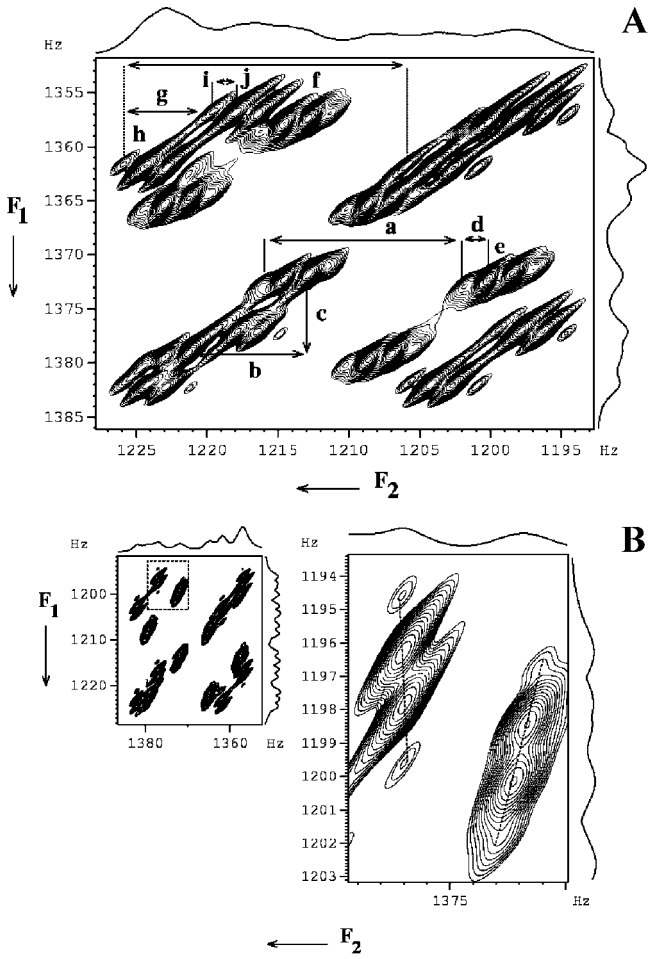

Figure 9. (A) The 500 MHz two-dimensional correlated spectra of a racemic mixture of (*R/S*)-propylene oxide with selective excitation of protons 6 and 7. The cross peaks at the chemical shift position of proton 7 are given in an expanded scale along with F_1 and F_2 projections. The width of the seduce shape pulse is 10 ms. The size of the 2D data matrix is 256 × 1024. Spectral widths are 250 and 320 Hz in the F_1 and F_2 dimensions. The number of accumulations for each t_1 increment is 4. The relaxation delay is 18 s. The data was zero-filled to 2048 and 4096 points and processed with a sine bell window function. The digital resolution in the F_1 and F_2 dimensions is 0.12 and 0.08 Hz. The separations marked with a, b, c, d, and e provide $^2T_{H6H7}$, $^3T_{H5H7}$, $^4T_{H5H6}$, $^3T_{H4H7}$, and $^3T_{H4H6}$ for the *S* enantiomer, and the separations marked with f, g, h, i, and j provide $^2T_{H6H7}$, $^3T_{H5H7}$, $^4T_{H5H6}$, $^3T_{H4H7}$, and $^3T_{H4H6}$ for the *R* enantiomer. (B) The cross peaks at the chemical shift position of proton 6 along with F_1 and F_2 projections. The expanded plot of the cross peaks marked with a broken rectangle shows the opposite direction of the tilt of the displacement vector, indicating the long-range passive coupling $^4T_{H4H7}$ is opposite in sign to other couplings. Similarly, the sign of the long-range coupling $^4T_{H4H6}$ is found to be opposite to others.

Those marked a and b provide $(^2T_{H4H4})^R$ and $(^3T_{H4H5})^R$, respectively, and c provides $(^4T_{H4H6})^R$ or $(^4T_{H4H7})^R$. Similarly, d and e provide $(^2T_{H4H4})^S$ and $(^3T_{H4H5})^S$, respectively, and f provides $(^4T_{H4H6})^S$ or $(^4T_{H4H7})^S$. Although the spectrum distinguishes the enantiomers and permits the determination of couplings, it does not identify the individual couplings, $^4T_{H4H6}$ and $^4T_{H4H7}$. Nevertheless, the information on four of the seven possible independent couplings could be obtained from this spectrum. However, the analysis is incomplete unless the couplings among the protons numbered 5, 6, and 7 (M, N and X spins), which are not reflected in either dimension, and the individual values of $^4T_{H4H6}$ and $^4T_{H4H7}$ are determined. The properly chosen selective excitation experiments of any of the two coupled protons numbered 5, 6, and 7 fills this lacuna.

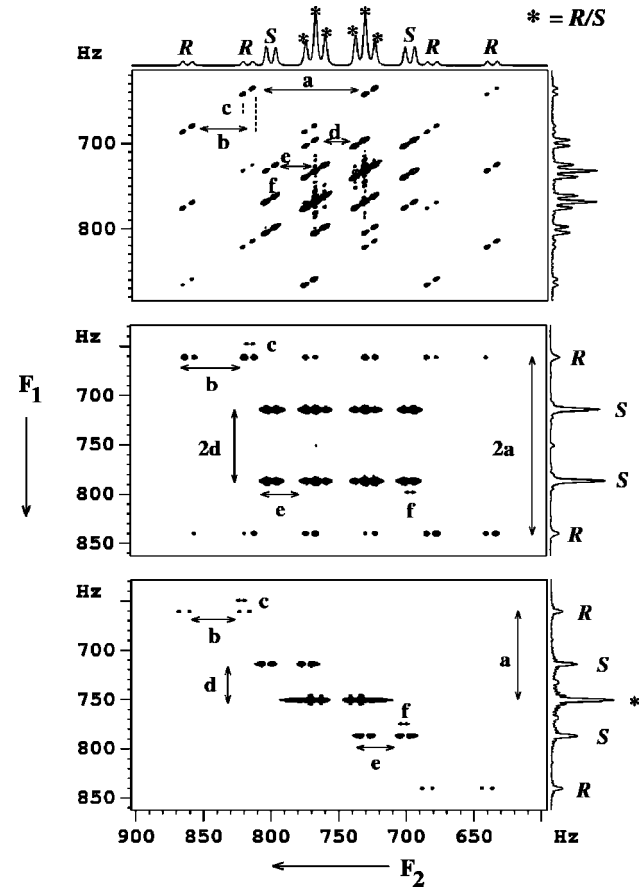

Figure 10. From the bottom trace to the top trace: The two-dimensional SERF, DQ-SERF, and Soft-COSY spectra of **2**, respectively, plotted on an identical scale for comparison. For the Soft-COSY experiment, the width of the shaped pulses, used for excitation and mixing periods EBURP-2 and UBURP, is 6.25 ms. The 2D data matrix size is 400 × 1024. Spectral widths are 300 and 350 Hz in the F_1 and F_2 dimensions, respectively. The number of accumulations for each t_1 increment is 4. The relaxation delay is 12.5 s. The data was zero-filled to 2048 and 4096 and processed with a sine bell window function. The digital resolution in the F_1 and F_2 dimensions is 0.15 and 0.09 Hz. For the DQ-SERF experiment, the width of the seduce shape pulse is 5.0 ms. The 2D data matrix size is 400 × 1024. Spectral widths are 350 Hz in both F_1 and F_2 dimensions. The number of accumulations for each t_1 increment is 4. The relaxation delay is 4.0 s. The data was zero-filled to 2048 and 4096 points and processed with a sine bell window function. The digital resolution in the F_1 and F_2 dimensions is 0.17 and 0.09 Hz. The optimized τ delay is 15.6 ms. For the SERF experiment, the shape pulses used for excitation and refocusing are EBURP-2 and REBURP, with widths of 10.0 ms. The 2D data matrix size is 206 × 1024. Spectral widths are 300 and 350 Hz in both F_1 and F_2 dimensions. The number of accumulations for each t_1 increment is 4. The relaxation delay is 12.5 s. The data was zero-filled to 1024 and 4096 points and processed without any window function. The digital resolution in the F_1 and F_2 dimensions is 0.3 and 0.1 Hz. The peaks from each enantiomer in the indirect dimensions are marked for both SERF and DQ-SERF spectra. However, for the Soft-COSY spectra, they are marked in the direct dimension, and the spectrum is symmetrical about the diagonal. The separations marked a, b, and c provide $^nT_{HH}$ (n = 2, 3, and 5) for the *R* enantiomer, and those marked d, e, and f provide $^nT_{HH}$ (n = 2, 3, and 5) for the *S* enantiomer. The peak with negligible intensity at the centre of the indirect dimension in the DQ-SERF experiment is due to an artifact whose origin is unknown. The peaks marked * in the indirect dimension of SERF and in the direct dimension of the Soft-COSY experiment indicate the overlap of transitions from both of the enantiomers. Detailed discussion of these spectra is reported in the text.

Figure 8A shows the 2D correlated spectrum of **3** (racemic mixture), with selectively excited protons 5 and 7, along with

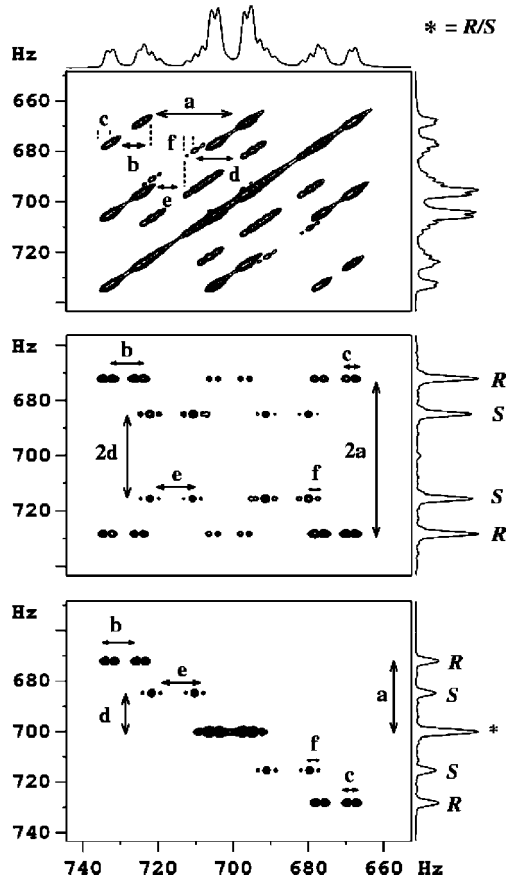

Figure 11. From the bottom trace to the top trace: 500 MHz two-dimensional SERF, DQ-SERF, and Soft-COSY spectra of the scalemic mixture of **3**, respectively, plotted on an identical scale for comparison. The peaks for the enantiomers are marked. For the Soft-COSY experiment, the width of the seduce shape pulse is 10.0 ms. The 2D data matrix size is 512 × 900. Spectral widths are 250.0 Hz in both the F_1 and F_2 dimensions. The number of accumulations for each t_1 increment is 4. The relaxation delay is 12.5 s. The data was zero-filled to 2048 and 4096 and processed with a sine bell window function. The digital resolution in the F_1 and F_2 dimensions is 0.12 and 0.06 Hz. Assignments for *R* and *S* are from the literature.[20] The separations marked with a, b, and c provide couplings $^2T_{H4H4}$, $^3T_{H4H5}$, and $^4T_{H4H6}$ or $^4T_{H4H7}$ for the *R* enantiomer and the separations d, e, and f provide $^2T_{H4H4}$, $^3T_{H4H5}$, and $^4T_{H4H6}$ or $^4T_{H4H7}$ for the *S* enantiomer. For the DQ-SERF experiment, the width of the seduce shape pulse is 5.0 ms. The 2D data matrix size is 256 × 600. Spectral widths are 150 and 200 Hz in the F_1 and F_2 dimensions, respectively. The number of accumulations for each t_1 increment is 4. The relaxation delay is 4.0 s. The data was zero-filled to 1024 and 2048 points and processed with a sine bell window function. The digital resolution in the F_1 and F_2 dimensions is 0.15 and 0.10 Hz. The optimized τ delay is 3.1 ms. For the SERF experiment, the shaped pulses employed are EBURP2 and REBURP for excitation and refocusing, with widths of 10.0 ms each. The 2D data matrix size is 342 × 900. Spectral widths are 250.0 Hz in both the F_1 and F_2 dimensions. The number of accumulations for each t_1 increment is 4.0 The relaxation delay is 12.5 s. The data was zero-filled to 1024 and 2048 points and processed with a sine bell window function. The digital resolution in the F_1 and F_2 dimensions is 0.24 and 0.12 Hz, respectively.

F_1 and F_2 projections. The spectrum provides one active coupling, $^3T_{H5H7}$, and four passive couplings, $^2T_{H6H7}$, $^3T_{H5H6}$, $^3T_{H4H5}$, and $^4T_{H4H7}$. The active coupling between one of the methylene and methine protons is obtainable along the F_2 dimension at the chemical sites of both protons 6 and 7, which is a doublet of identical separation.

The expanded plot pertaining to cross peaks of proton 7 (marked with a broken rectangle in Figure 8A) is given in Figure 8B. The passive coupling of this proton with the geminal proton 6 splits its resonance into a doublet of larger separation ($^2T_{H6H7}$), which is further split into a doublet from a methine proton ($^3T_{H5H7}$). Each component of the doublet of the doublet is split into a quartet from methyl protons ($^4T_{H4H7}$). Thus, the F_2 dimension provides four sets of quartets, which are displaced according to two passive couplings $^4T_{H4H7}$ and $^2T_{H6H7}$. The F_1 displacement provides two other passive couplings $^3T_{H5H6}$ and $^3T_{H4H5}$. The resolution of the quartet due to long-distance coupling $^4T_{H4H7}$ is exceptionally good. One such quartet for each enantiomer is shown by joining the peaks with a tilted line. The couplings obtainable from the displacement vectors are marked in Figure 8B. This dramatically enhanced resolution permits the measure of the coupling on the order of 0.6 Hz for the *R* enantiomer. The separations marked with solid lines and represented by a, b, c, d, and e, respectively, provide $(^3T_{H5H7})^R$, $(^2T_{H6H7})^R$, $(^4T_{H4H7})^R$, $(^3T_{H5H6})^R$, and $(^3T_{H4H5})^R$. Similarly, separations marked with broken lines and represented by g, h, i, j, and k, respectively, provide $(^3T_{H5H7})^S$, $(^2T_{H6H7})^S$, $(^4T_{H4H7})^S$, $(^3T_{H5H6})^S$, and $(^3T_{H4H5})^S$. F_1 displacement also provides $(^3T_{H5H7})^R$ and $(^3T_{H5H7})^S$. This information is redundant and is not marked. From the cross-peak region of the spectrum corresponding to proton 5 (Figure 8A), similar information is obtainable. However, the values of $(^4T_{H4H6})^{R/S}$ could not be determined precisely by this experiment. Another experiment with the selective excitation of protons 6 and 7 (spectrum not shown) provided the above-mentioned couplings and $(^4T_{H4H6})^{R/S}$ instead of $(^4T_{H4H7})^{R/S}$. Thus, the values of $(^4T_{H4H6})^{R/S}$ and $(^4T_{H4H7})^{R/S}$ could be determined independently combining the two experiments. Thus, the combination of three spin-selective correlation experiments provided the totality of the coupling information for this molecule. All of the determined parameters are given in Table 1. These parameters would have been otherwise impossible to obtain from the broad and featureless one-dimensional spectrum.

Because of the identical spin system and similar multiplet pattern, the analyses of the spectrum of **4** can be carried out in exactly the same way as that of **3**. The 2D correlated spectrum of **4** with selective excitation of the methyl protons, shown in top trace of Figure 12, is also significantly simplified. However, the small strength of remote couplings results in loss of resolution. The separations giving $(^2T_{H4H4})^{R/S}$ and $(^3T_{H4H5})^{R/S}$ and $(^4T_{H4H6})^{R/S}$ and $(^4T_{H4H7})^{R/S}$ could be obtained for both enantiomers, which are marked with a−f.

The two-dimensional correlated spectrum of selectively excited protons 6 and 7 of **4** is reported in Figure 9. The analysis of this spectrum is similar to that of **3** shown in Figure 8. The resolution achieved is dramatic, which is clearly evident from the marked separations. The parameters $(^3T_{H6H5})^{R/S}$ and $(^4T_{H4H6})^S$ could be determined from the displacement vectors. The two different $(^4T_{H4H6})^{R/S}$ and $(^4T_{H4H7})^{R/S}$ could be unambiguously derived. The $(^2T_{H6H7})^{R/S}$ between geminal protons of the methylene group was also extracted directly from the F_2 cross section. Even though the one-dimensional proton spectrum of **4** is broader and featureless compared to that of **3**, the selectively correlated spectrum gave well-resolved cross peaks for both *R* and *S* enantiomers. One additional feature of this spectrum is the relative signs of the coupling, which will be discussed later.

Comparison of SERF, DQ-SERF, and Soft-COSY Experiments. The selective methyl-proton-excited SERF, DQ-SERF, and Soft-COSY spectra of **2**, plotted on an identical scale, are compared in Figure 10. The separations providing the information on $^nT_{HH}$ (n = 2, 3, and 5) in all three types of spectra are marked a, b, and c for the *R* enantiomer and d, e, and f for the

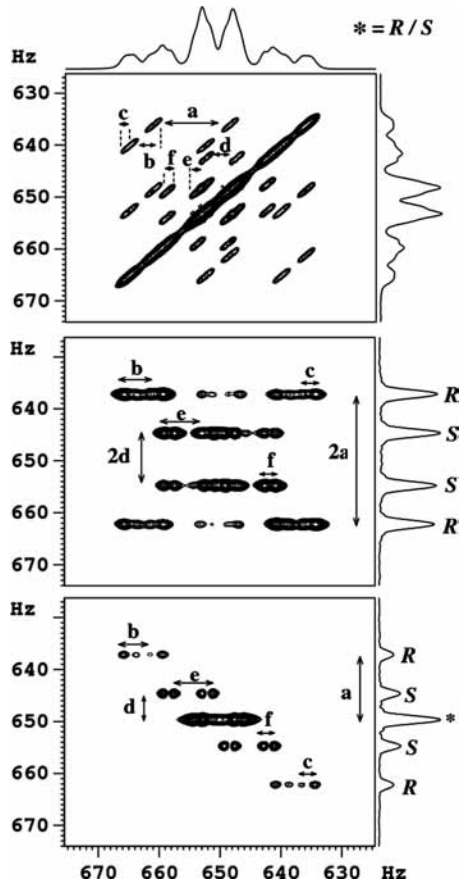

Figure 12. From the bottom trace to the top trace: The two-dimensional SERF, DQ-SERF, and Soft-COSY spectra of **4**, respectively, plotted on an identical scale for comparison. For the Soft-COSY experiment, the shape pulses employed for excitation and mixing are EBURP2 and UBURP, with respective widths of 8.3 and 10.0 ms. The 2D data matrix size is 200 × 450. Spectral widths are 75.0 and 100 Hz in the F_1 and F_2 dimensions, respectively. The number of accumulations for each t_1 increment is 4. The relaxation delay is 18.0 s. The data was zero-filled to 1024 and 2048 and processed with a sine bell window function. The digital resolution in the F_1 and F_2 dimensions is 0.07 and 0.04 Hz. The separations marked with a, b, and c provide coupling information $^2T_{H4H4}$, $^3T_{H4H5}$, and $^4T_{H4H6}$ or $^4T_{H4H7}$ for the *R* enantiomer, and the separations d, e, and f and provide information $^2T_{H4H4}$, $^3T_{H4H5}$, and $^4T_{H4H6}$ or $^4T_{H4H7}$ for the *S* enantiomer. For the DQ-SERF experiment, the width of the seduce shape pulse is 8.3 ms. The 2D data matrix size is 128 × 340. Spectral widths are 65 and 100 Hz in the F_1 and F_2 dimensions, respectively. The number of accumulations for each t_1 increment is 4. The relaxation delay is 18.0 s. The data was zero-filled to 1024 and 2048 points and processed with a sine bell window function. The digital resolution in the F_1 and F_2 dimensions is 0.06 and 0.05 Hz. The optimized τ delay is 7.0 ms. For the SERF experiment, the shape pulses used are EBURP-2 and REBURP for excitation and refocusing, with widths of 8.3 and 10.0 ms, respectively. The 2D data matrix size is 128 × 474. Spectral widths are 65.0 and 140 Hz in the F_1 and F_2 dimensions. The number of accumulations for each t_1 increment is 4. The relaxation delay is 18.0 s. The data was zero-filled to 1024 and 2048 points and processed with a sine bell window function. The digital resolution in the F_1 and F_2 dimensions is 0.06 and 0.07 Hz. The peaks from each enantiomer in the indirect dimensions are marked for SERF and DQ-SERF spectra. However, for the Soft-COSY spectra, they are marked in the direct dimension, and the spectrum is symmetrical about the diagonal. The separations marked a, b, and c provide $^nT_{HH}$ ($n = 2$, 3, and 4) for the *R* enantiomer, and those marked d, e, and f provide $^nT_{HH}$ ($n = 2$, 3, and 4) for the *S* enantiomer. The peaks marked * in the indirect dimension of SERF indicate the overlap of transitions from both enantiomers. Detailed discussion of these spectra is reported in the text.

S enantiomer. The visualization of enantiomers is evidently obvious in all three experiments.

In the indirect dimension of the SERF experiment, the separation of the adjacent transitions of the triplet of each enantiomer provides couplings between the active spins (short-distance coupling, $^2T_{HH}$). The direct dimension provides the coupling between active and passive spins (long-distance couplings,$^3T_{HH}$ and $^5T_{HH}$). However, the central peak of the methyl triplet does not precess in the indirect dimension, resulting in their overlap from both of the enantiomers, implying that there is no complete spectral discrimination. Nevertheless, the SERF experiment has been demonstrated to be useful in quantifying enantiomeric excess by measuring the integrals of the F_1 cross sections and also by the 3D volume of the contours.[16]

In DQ-SERF, on the other hand, there is a complete separation of the overlapped spectra of methyl peaks for each enantiomer, both in the DQ as well as in the SQ dimensions, thereby overcoming the problem of this overlap. The DQ dimension provides a doublet corresponding to two spin states of the passive methyl proton, unlike a triplet in SERF. The separation between the two transitions of the doublet provides information on the short-distance coupling for each enantiomer. However, this separation is twice (2 X $^2T_{HH}$) compared to the SERF experiment, thereby enhancing the resolution by a factor of 2, resulting in better chiral discrimination. Furthermore, the cross section taken parallel to the SQ dimension at each spin state of an enantiomer pertains to the fully coupled spectrum corresponding to a methyl group of an enantiopure compound. This is because the transitions are not spin-state-selected and the active and passive couplings are not separated in two dimensions. Thus, although the information on all of the couplings, including the short-distance coupling between the methyl protons, can be derived from any one of these cross sections, the spectral complexity still persists. Furthermore, for exciting maximum coherence from both of the enantiomers in the DQ dimension, the τ delay is required to be optimized, which causes nonuniform excitation. This is a severe drawback as far as the quantitative measurement of enantiomeric excess is concerned.

In Soft-COSY, the spectra being symmetric, all of the coupling information ($^nT_{HH}$) is derivable in both direct and indirect dimensions. The significant advantage of this experiment over the two previous experiments lies in its spin state selection. In the 2D data matrix, the F_2 dimension reveals the coupling between the active spins, and the displacement of arrays in the F_1 dimension reveals the passive couplings. This removes spectral complexity in each cross section, unlike that in DQ-SERF. This advantage is obvious from the top trace of Figure 10. Additionally, several overlapped transitions (marked * in the SQ dimension) of both of the enantiomers get separated in both dimensions. As discussed previously, a few consecutive cross sections (only three cross sections in (*R*/*S*)-3-butyn-2-ol) taken parallel to the SQ dimension is sufficient for the determination of all of the coupling parameters. The resolution of the spectra with a racemic mixture (Figure 5) is better than that with the scalemic mixture (top trace of Figure 10). Nevertheless, the Soft-COSY could resolve all of the peaks pertaining to both enantiomers. The significant advantage of Soft-COSY is once again demonstrated in this spectrum. The derived couplings for both scalemic and racemic mixtures are given in Table 1. A similar comparison of the spectra with selective excitation of the methyl protons in **3** and **4** is made in Figures 11 and 12, respectively. The unambiguous enantiomeric visualization, separation of the short- and long-distance couplings, and the spin state selection in Soft-COSY are clearly evident in both of these spectra.

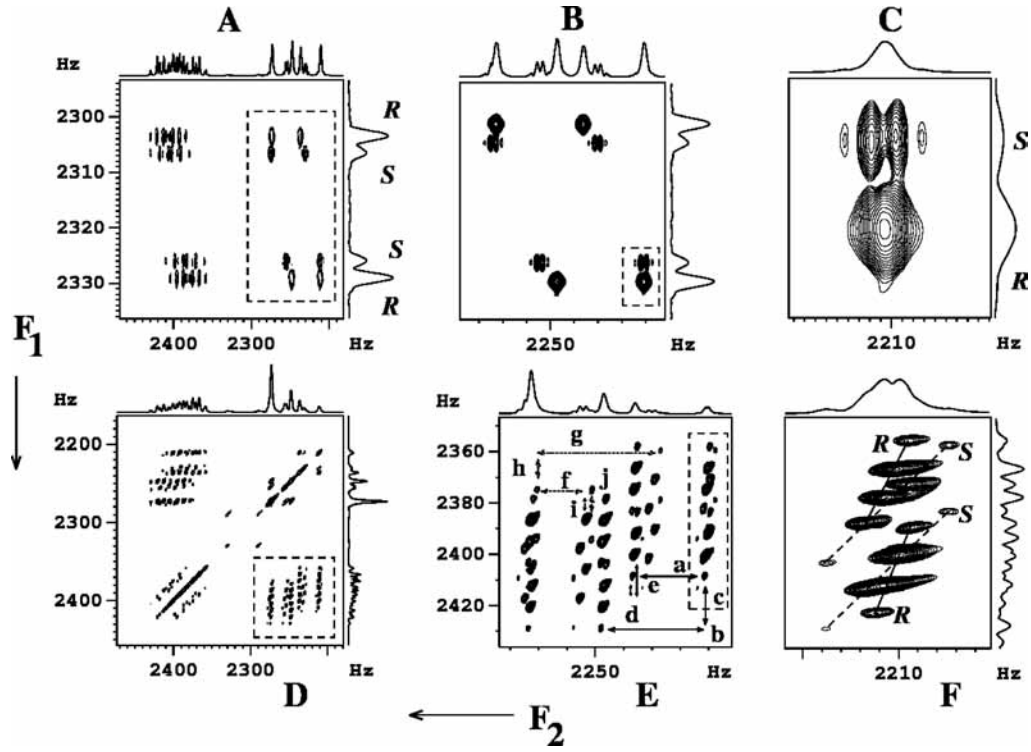

Figure 13. (A−C) Two-dimensional SERF and (D−F) two-dimensional Soft-COSY spectra of a scalemic mixture of **3**, where the protons numbered 5 and 7 are simultaneously excited using a selective pulse. B and E are the expanded plots of the rectangles depicted with broken lines in A and D. C and F depict further expansion of the marked regions in B and E.

Advantages and Limitations of the Spin-Selected Correlation Experiments. The biggest advantage of the Soft-COSY experiment, which is not obvious from this selective methyl-excited experiment, is in the selective excitation of two protons. When appropriately chosen, two or three such experiments provide magnitudes of all of the proton−proton couplings in addition to their relative signs. Since the specific region of the spectrum is selectively excited, the resolution of the spectrum is dramatically enhanced due to smaller spectral width. This is distinctly brought out in Figure 13, where the SERF (A−C) and Soft-COSY (D−E) spectra of the scalemic mixture of **3** are compared. Both SERF and Soft-COSY spectra are with the selective excitation of protons numbered 5 and 7. The expanded regions marked in rectangles with a broken line demonstrate the resolution achievable in Soft-COSY. For better clarity, the regions of Figure 13A and D are given with expansions in Figure 13B and E. The two sets of quartets arising from both *R* and *S* enantiomers due to long-distance couplings (on the order of 2.1 Hz) with methyl protons are clearly distinguishable in Soft-COSY. On the other hand, SERF resolves the quartet of the *S* enantiomer only (Figure 13C). For the *R* enantiomer, the long-range coupling is on the order of 0.6 Hz, which is resolved only in Soft-COSY (Figure 13F). With such incredible resolution achieved due to displacement of peaks in the F_1 dimension, it is possible to measure couplings smaller than line widths in Soft-COSY, whereas it is impossible to derive these couplings from the SERF experiment. The coupling strength of 0.2 Hz (Table 2) determined using Soft-COSY from the broad and featureless spectra of (*R*/*S*)-propylene oxide further supports this conclusion. The resolution of the spectra of **2** with a racemic mixture (Figure 5) is better than that of the scalemic mixture (top trace of Figure 10). Nevertheless, the Soft-COSY could resolve all of the peaks pertaining to both of the enantiomers. The significant advantage of Soft-COSY is once again demonstrated in this spectrum. Thus, the limitation of this experiment lies only in the natural line width.

TABLE 2: The quantification of enantiomeric excess from the measured 3D volumes of different contours marked rectangles with broken and solid sline in fig. 14, in (*R*/*S*)-3-butyn-2-ol and (*R*/*S*)-propylene carbonate

(*R*/*S*)-3-butyn-2-ol[a]		(*R*/*S*)-propylene carbonate[b]	
contour number	measured ee from 3D volume (%)	contour number	measured ee from 3D volume (%)
1.	17.7	1.	25.1
2.	17.5	2.	22.4
3.	26.8[c]	3.	26
4.	44.7[c]	4.	21.2

[a] Prepared sample was a scalemic mixture with 18.5% ee of *S* enantiomer. [b] Prepared sample was a scalemic mixture with 21.0% ee of *S* enantiomer. [c] There is an overlap from the nearby transitions due to spectral crowding, and the measured values for these contours are likely to be imprecise.

As far as the experimental time is concerned, there is enormous saving in the instrument time in the spin-selected correlation experiment compared to the nonselective COSY experiment. Each two-dimensional selectively excited correlated spectrum requires typically less than half of an hour (also depends on the T_1 relaxation delay), while the nonselective COSY spectrum, to achieve a similar resolution, requires several hours of the instrument time. In other words, all of the spectral parameters could be derived by several spin-selective correlation experiments in less than the total experimental time required for a single nonselective COSY experiment.

As far as chiral discrimination is concerned, the only requirement is that there should be a measurable differential ordering effect on the order sensitive NMR parameters. There is neither any limiting value of degree of ordering nor any requirement of its prior knowledge before selective excitation.

This has been confirmed by carrying out identical experiments on two samples prepared with different enantiomeric compositions which have different order parameters, that is, scalemic and racemic samples of **2** and **3**. The spectra were obtained with a similar resolution, and all of the couplings could be derived with the same precision. The couplings for both of these compositions are reported in Table 1. However, the molecules with numerous larger size couplings from several long- and short-distance protons might result in a severe overlap of transitions. Nevertheless, as long as there are isolated groups permitting selective excitation without disturbing the nearby resonances, it is possible to monitor the response of the spin systems and extract the desirable information. With the possibility of transition selective excitation in the present day spectrometers, this is no longer a hurdle.[30]

Relative Signs of the Couplings. From the direction of the tilt of the displacement vector, it is possible to determine the relative signs between active and passive couplings. If the spin systems are strongly coupled, the question of the determination of relative signs does not arise. Thus, the method is applicable when the spectra are first order, that is, spins that are weakly scalar coupled, weakly dipolar coupled in strongly orienting media, and weakly dipolar coupled in chiral or bicellar media. There are situations when the relative signs of the couplings determined from the direction of the tilt of the displacement vector could be ambiguous. We have carried out extensive experimental studies and theoretically understood the response of the spin systems and their complete dynamics in the selective excitation of both single and multiple quantum coherence when applied to weakly coupled spin systems in the strongly orienting media. The results of this study are yet to be communicated and are not relevant for the present discussion. However, it is sufficient to mention that the selectively methyl-proton-excited correlation experiments do not provide the relative signs of the couplings. On the other hand, in the biselective excitation of different spins, it is possible to determine the relative signs. Studies on the molecules **1**, **2**, and **3** reveal that all of the couplings have the same signs in each enantiomer. Interestingly in **4**, the tilt of the displacement vector shown in the expanded part of the cross peak in Figure 9B is opposite to that of other couplings. This indicates that the long-range couplings $(^4T_{H4H6})^R$ and $(^4T_{H4H7})^R$ have opposite signs compared to those of all of the other couplings of the *R* enantiomer, whereas in the *S* enantiomer, $(^4T_{H4H6})^S$ and $(^4T_{H4H7})^S$ have similar signs relative to those of all of the other couplings.

Quantification of Enantiomeric Excess. The intensities of the NMR peaks are employed for the quantitive measurement of mixtures.[31] When the excitation over a small bandwidth is uniform, the ratio of the intensities of the contours can be utilized to quantify the enantiomeric excess (ee). The selective methyl-proton-excited correlation spectra in **2** (scalemic mixture) (Figure 14 A) and the selective excited spectra of protons numbered 5 and 7 in **3** (scalemic mixture) (Figure 14B) on the samples with known scalemic composition were chosen for quantification. Four different contours, as reported in Figure 14, were chosen for the *R* enantiomer (rectangles with solid lines), and the corresponding contours were selected for the *S* enantiomer (rectangles with broken lines) in both **2** and **3** for measuring the enantiomeric excess. The 3D volumes for all of the chosen contours were measured using Bruker XwinNMR software. The areas of the contours for both of the molecules are reported in Table 2. The error in the measured ee was around 5% for some contours in both **2** and **3**. However, for some contours, the errors were enormously large, more so in the contour marked 4 in **2**, the reasons for which is still not clear; more investigations to optimize this methodology for the precise determination of the enantiomeric excess are in progress. Further investigations to extend this method to more complex molecules, for the determination of structures of individual enantiomers, to systematize the methodology with different excitation sequences, and the development of the phase-sensitive version of the present and different excitation sequences are in progress.

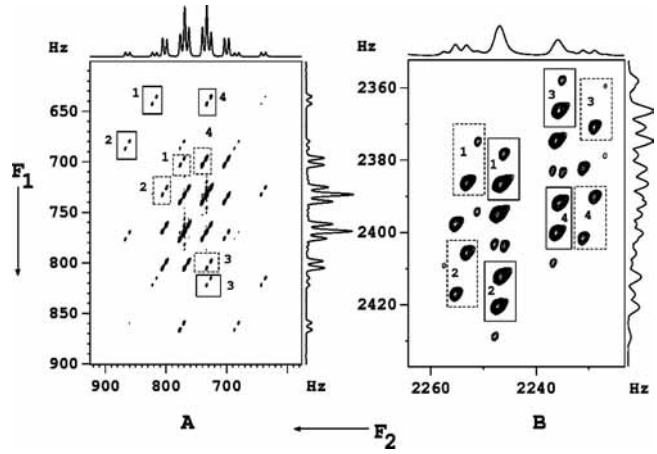

Figure 14. (A) Expanded region of the spectrum of the scalemic mixture of **2**, where methyl protons are selectively excited. (B) Expanded region of the spectrum of the scalemic mixture of **3**, where protons 5 and 7 are selectively excited. The four different contours chosen to quantify the enantiomeric excess are numbered and represented by rectangles with solid lines for the *R* enantiomer and with broken lines for the *S* enantiomer. The 3D volumes of these contours are reported in Table 2.

Conclusions

The present study employs the separation of active and passive couplings achieved by the two-dimensional ^{1}H NMR correlation of a selectively excited isolated group of coupled spins for unambiguous enantiomeric visualization, spectral simplification, and the determination of precise spectral parameters. The chiral molecules whose spectral complexity increases progressively with the number of interacting protons have been studied. All of the coupling parameters have been determined from the broad and featureless spectra, which are otherwise difficult to analyze and derive any meaningful information. The study also permits the determination of the relative signs of the couplings in systems whose NMR spectra are first order. The method also finds applications in weakly aligned systems like bicelles, scalar, or dipolar coupled systems in weakly or strongly orienting media. The method also may be used for quantification of the enantiomeric excess. Comparative study with other existing methods for enantiomeric visualization like SERF and DQ-SERF have been made and demonstrated the superiority of the spin-selected correlation experiment for such a purpose. For bigger molecules with an isolated group of coupled protons, an appropriate combination of experiments with different selective excitations may finally lead to complete spectral analysis. For the enantiomeric discrimination and determination of all of the proton−proton couplings with relative signs and magnitudes and the enantiomeric excess, Soft-COSY is a unique method compared to SERF and DQ-SERF. The study leads to routine employment of ^{1}H NMR studies for chiral discrimination, which was hitherto reported in the literature as difficult.

Acknowledgment. N.S. gratefully acknowledges the Department of Science and Technology, New Delhi, for the financial

Grant No. SR/S1/PC-13/2004 and U.R.P. and B.B. thank CSIR, India, for a fellowship.

References and Notes

(1) Lesot, P.; Merlet, D.; Courtieu, J.; Emsley, J. W.; Rantala, T. T.; Jokisaari, J. *J. Phys. Chem. A* **1997**, *101*, 5719–5724.
(2) Lesot, P.; Lafon, O.; Courtieu, J.; Berdagué, P. *Chem.—Eur. J.* **2004**, *10*, 3741–3746.
(3) Canet, I.; Courtieu, J.; Loewenstein, A.; Meddour, A.; Péchiné, J. M. *J. Am. Chem. Soc.* **1995**, *117*, 6520–6526.
(4) Lafon, O.; Lesot, P.; Merlet, D.; Courtieu, J. *J. Magn. Reson.* **2004**, *171*, 135–142.
(5) Merlet, D.; Sarfati, M.; Ancian, B.; Courtieu, J.; Lesot, P. *Phys. Chem. Chem. Phys.* **2000**, *2*, 2283–2290.
(6) Lesot, P.; Merlet, D.; Loewenstein, A.; Courtieu, J. *Tetrahedron: Asymmetry* **1998**, *9*, 1871–1881.
(7) Merlet, D.; Ancian, B.; Smadja, W.; Courtieu, J.; Lesot, P. *Chem. Commun.* **1998**, 2301–2302.
(8) Merlet, D.; Ancian, B.; Courtieu, J.; Lesot, P. *J. Am. Chem. Soc.* **1999**, *121*, 5249–5258.
(9) Lesot, P.; Lafon, O.; Courtieu, J.; Berdagué, P. *Chem.—Eur. J.* **2004**, *10*, 3741–3746.
(10) Meddour, A.; Berdagué, P.; Hedli, A.; Courtieu, J.; Lesot, P. *J. Am. Chem. Soc.* **1997**, *119*, 4502–4508.
(11) Madiot, V.; Lesot, P.; Grée, D. *Chem. Comm.* **2000**, *16*, 9–170.
(12) Jakubcova, M.; Meddour, A.; Péchiné, J. M.; Baklouti, A.; Courtieu, J. *J. Flourine Chem.* **1997**, *86*, 149–153.
(13) Sarfati, M.; Lesot, P.; Merlet, D.; Courtieu, J. *Chem. Commun.* **2000**, 2069–2081.
(14) Lounila, J.; Jokisaari, J. *Prog. Nucl. Magn. Reson. Spectros.* **1982**, *15*, 249–290.
(15) Uday, R. P.; Bikash, B.; Suryaprakash, N. *J. Magn. Reson.* **2008**, *191*, 259–266.
(16) Farjon, J.; Merlet, D.; Lesot, P.; Courtieu, J. *J. Magn. Reson.* **2002**, *158*, 169–172.
(17) Beguin, L.; Courtieu, J.; Ziani, L.; Merlet, D. *Magn. Reson. Chem.* **2006**, *44*, 1096–1101.
(18) Lesot, P.; Merlet, D.; Courtieu, J.; Emsley, J. W. *Liq. Cryst.* **1996**, *21*, 427–435.
(19) Farjon, J.; Baltaze, J. P.; Lesot, P.; Merlet, D.; Courtieu, J. *Magn. Reson. Chem.* **2004**, *42*, 594–599.
(20) Ziani, L.; Courtieu, J.; Merlet, D. *J. Magn. Reson.* **2006**, *183*, 60–67.
(21) Marathias, M.; Goljer, I.; Bach, A. C., II *Magn. Reson. Chem.* **2005**, *43*, 512–519.
(22) Marathias, M.; Tawa, G. J.; Goljer, I.; Bach, A. C., II *Chirality* **2007**, *19*, 741–750.
(23) Bikash, B.; Uday, R. P.; Suryaprakash, N. *J. Phys. Chem. B* **2007**, *111*, 12403–12410.
(24) Brüschweiler, R.; Madsen, J. C.; Griesinger, C.; Sørensen, O. W.; Ernst, R. R. *J. Magn. Reson.* **1987**, *73*, 380–385.
(25) Emsley, L.; Bodenhausen, G. *J. Magn. Reson.* **1989**, *82*, 211.
(26) Cavanagh, J.; Waltho, J. P.; Keeler, J. *J. Magn. Reson.* **1987**, *74*, 386.
(27) Emsley, L. *Methods Enzymol.* **1994**, *239*, 207–246.
(28) Griesinger, C.; Sørensen, O. W.; Ernst, R. R. *J. Am. Chem. Soc.* **1985**, *107*, 6394–6396.
(29) Griesinger, C.; Sørensen, O. W.; Ernst, R. R. *J. Chem. Phys.* **1986**, *85*, 6837–6852.
(30) Mahesh, T. S.; Dorai, K.; Kumar, A.; Kumar, A. *J. Magn. Reson.* **2001**, *148*, 95–103.
(31) Giraudeau, P.; Guignard, N.; Hillion, E.; Baguet, E.; Akoka, S. *J. Pharm Biomed. Anal.* **2007**, *43*, 1243–1248.

JP7102462